

Neutron Spin Resonance in the 112-Type Iron-Based Superconductor

Tao Xie,^{1,2} Dongliang Gong,^{1,2} Haranath Ghosh,^{3,4} Abyay Ghosh,^{3,4} Minoru Soda,⁵ Takatsugu Masuda,⁵ Shinichi Itoh,⁶ Frédéric Bourdarot,⁷ Louis-Pierre Regnault,⁸ Sergey Danilkin,⁹ Shiliang Li,^{1,2,10} and Huiqian Luo^{1,*}

¹*Beijing National Laboratory for Condensed Matter Physics,
Institute of Physics, Chinese Academy of Sciences, Beijing 100190, China*

²*University of Chinese Academy of Sciences, Beijing 100049, China*

³*Homi Bhabha National Institute, Anushakti Nagar, Mumbai 400094, India*

⁴*Human Resources development section, Raja Ramanna Centre for Advanced Technology, Indore - 452013, India*

⁵*The Institute for Solid State Physics, The University of Tokyo, Chiba 277-8581, Japan*

⁶*Institute of Materials Structure Science, High Energy Accelerator Research Organization, Tsukuba, Ibaraki 305-0801, Japan*

⁷*Université Grenoble Alpes, CEA, INAC, MEM MDN, F-38000 Grenoble, France*

⁸*Intitut Laue Langevin, 71 avenue des Martyrs, CS 20156, 38042 Grenoble Cedex, France*

⁹*Australian Centre for Neutron Scattering, Australian Nuclear Science
and Technology Organization, Lucas Heights NSW-2234, Australia*

¹⁰*Collaborative Innovation Center of Quantum Matter, Beijing 100190, China*

(Dated: September 11, 2018)

We use inelastic neutron scattering to study the low-energy spin excitations of the 112-type iron pnictide $\text{Ca}_{0.82}\text{La}_{0.18}\text{Fe}_{0.96}\text{Ni}_{0.04}\text{As}_2$ with bulk superconductivity below $T_c = 22$ K. A two-dimensional spin resonance mode is found around $E = 11$ meV, where the resonance energy is almost temperature independent and linearly scales with T_c along with other iron-based superconductors. Polarized neutron analysis reveals the resonance is nearly isotropic in spin space without any L modulations. Because of the unique monoclinic structure with additional zigzag arsenic chains, the As $4p$ orbitals contribute to a three-dimensional hole pocket around the Γ point and an extra electron pocket at the X point. Our results suggest that the energy and momentum distribution of the spin resonance does not directly respond to the k_z dependence of the fermiology, and the spin resonance intrinsically is a spin-1 mode from singlet-triplet excitations of the Cooper pairs in the case of weak spin-orbital coupling.

PACS numbers: 74.70.Xa, 75.30.Gw, 78.70.Nx, 75.40.Gb

In unconventional superconductors such as copper oxides, heavy fermions, and iron-based superconductors, the neutron spin resonance is a crucial evidence for spin fluctuation mediated superconductivity in the proximity of an antiferromagnetic (AF) instability. On cooling below the superconducting transition temperature T_c , the intensity of spin excitations around a particular energy (the so called resonance energy E_R) behaves like a superconducting order parameter [1–5]. Theoretically, the spin resonance mode is generally believed to be a spin-1 exciton from the singlet-triplet excitations of the electron Cooper pairs [6–9]. However, such a picture is still not well established yet in the iron-based superconductors, although the spin resonance has been observed in many superconducting iron pnictides and iron chalcogenides [4, 5, 10–32]. The spin resonance is argued to arise from the sign-reversed ($s\pm$) quasiparticle excitations between different Fermi surfaces in these multiband systems [33–35]. Such a mechanism should yield a sharp resonant peak with an energy below the total superconducting gaps summed on the nesting bands [9, 26, 33], while some exceptions in particular compounds with a broad enhancement of intensity and $E_R > 2\Delta$ are argued to be the sign-preserved (s_{++}) superconducting state [27–32]. The proximity to the AF order and spin-orbital coupling give further complexity on the energy and momentum distribution of spin resonance [12–21]. Similar to the cuprate

superconductors, the resonance energy in iron-based superconductors overall follows a linear scaling with T_c with slightly different prefactor: $E_R \approx 4.9k_B T_c$, suggesting the common features of the magnetism in various materials and their intimate relation to high- T_c superconductivity [Fig. 1(d)] [5, 9, 10, 30, 36, 37].

The 112-type iron pnictide $\text{Ca}_{1-x}\text{La}_x\text{FeAs}_2$ discovered in 2013 has a unique noncentrosymmetric lattice structure derivative from HfCuSi_2 with additional zigzag arsenic chains between Ca/La layers [38, 39]. Its magnetic order is very similar to the collinear antiferromagnetism in BaFe_2As_2 (122 type) or NaFeAs (111 type) with same wavevector $\mathbf{Q}_{AF} = (1, 0)$ in the unit cell with two Fe atoms (or $\mathbf{Q} = (0.5, 0.5)$ in the one Fe unit cell), but the ordered moments are 45° away from the easy axis of the stripe direction along a_M [Fig. 1(a)] [1, 5, 10, 39]. Comparing to other iron-based superconductors, the fermiology of $\text{Ca}_{1-x}\text{La}_x\text{FeAs}_2$ is also composed of two hole pockets at the zone center (Γ point) and one oval-like electron pocket at the zone corner (M point) [39, 41]. However, one additional 3D hole pocket around Γ point and one more electron pocket at the Brillouin zone edge (X point) are contributed by $4p$ orbitals from As chains in hybridization with Fe $3d$ orbitals [42, 43]. While filamentary superconductivity can be obtained in the pure La doped compounds [41, 44–46], further doping Co or Ni can improve the system to bulk superconductivity

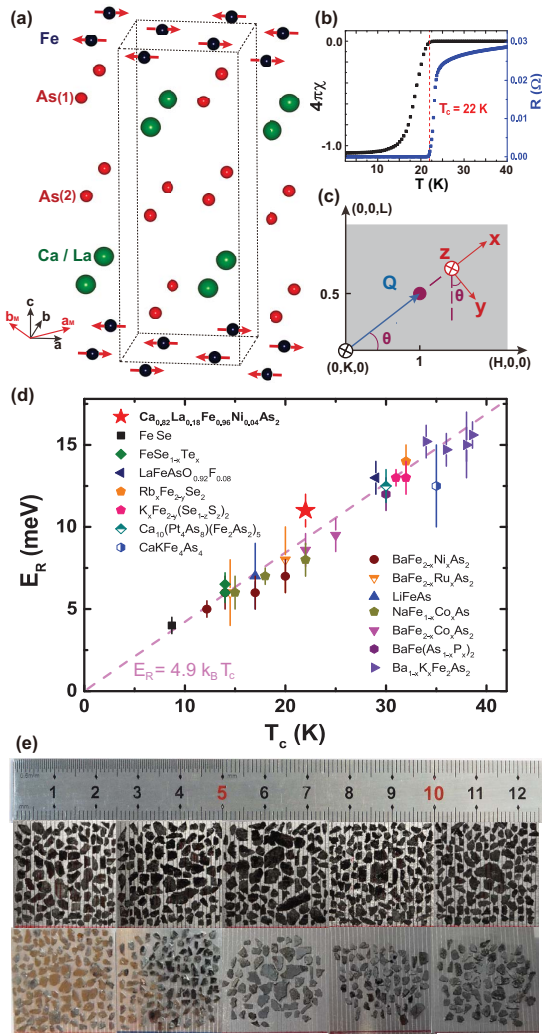


FIG. 1: (a) Crystal and magnetic structure of the $\text{Ca}_{1-x}\text{La}_x\text{FeAs}_2$ system. (b) Superconducting transitions of our $\text{Ca}_{0.82}\text{La}_{0.18}\text{Fe}_{0.96}\text{Ni}_{0.04}\text{As}_2$ samples measured by the resistivity and magnetic susceptibility. (c) Polarization setup in the reciprocal space for the polarized neutron scattering experiment. (d) Linear scaling between the resonance energy E_R and critical temperature T_c in iron-based superconductors [5, 12–16, 18–26, 28, 29, 32, 36, 37]. (e) Photo of the coaligned $\text{Ca}_{0.82}\text{La}_{0.18}\text{Fe}_{0.96}\text{Ni}_{0.04}\text{As}_2$ crystals.

with T_c up to 34 K [1, 47]. Unlike the nearly isotropic superconductivity in the 122 system [48], transport experiments reveal a quasi-2D behavior of superconducting fluctuations in the 112 system [49].

Here, in this letter, we report a systematic inelastic neutron scattering study on the 112-compound $\text{Ca}_{0.82}\text{La}_{0.18}\text{Fe}_{0.96}\text{Ni}_{0.04}\text{As}_2$ with bulk superconductivity below $T_c = 22$ K [Fig. 1(b)]. We have found a 2D spin resonance in reciprocal space with resonance energy $E_R = 11$ meV in scaling with other iron-based superconductors [Fig. 1(d)] [4–29]. Polarized neutron analysis reveals that the resonance is isotropic in spin space due to

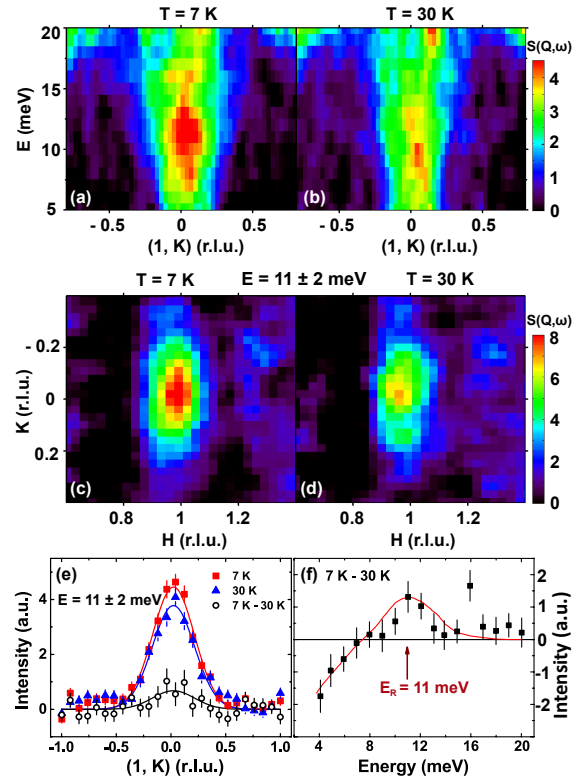


FIG. 2: (a), (b) Energy dependence of the two-dimensional slices along the $\mathbf{Q} = (1, K)$ direction with $E_i = 40$ meV at $T = 7$ and 30 K. (c), (d) Constant-energy slices of the magnetic excitations with $E = 11 \pm 2$ meV at $T = 7$ and 30 K. (e) One-dimensional cuts of the magnetic excitations at $E = 11 \pm 2$ meV along the $\mathbf{Q} = (1, K)$ direction. The red and blue lines are Gaussian fits to the raw data, and the black line is their difference. (f) Spin resonance mode revealed by the difference of the spin excitations between $T = 7$ and 30 K. The solid lines are guides to the eyes.

weak spin-orbit coupling. After comparing with the calculated band structure and Fermi surfaces, we conclude that the spin resonance mode in the 112 system is intrinsically from spin singlet-triplet excitations, and it does not directly respond to the 3D Fermi surface induced by the As $4p$ orbitals.

We prepared high quality single crystals of $\text{Ca}_{0.82}\text{La}_{0.18}\text{Fe}_{0.96}\text{Ni}_{0.04}\text{As}_2$ using the self-flux method [1] and coaligned 2.3 g single crystals [about 1500 pieces, see Fig. 1(e)] with a small mosaic about 4° in the ab plane and 3° along the c axis [50]. The transport characterization suggests the superconducting transition is very sharp with $T_c = 22$ K and about a 100% shielding volume at low temperature [Fig. 1(b)]. Time-of-flight neutron scattering experiments were carried out at the HRC spectrometer (BL-12) at J-PARC, Tokai, Japan, with an incident energy $E_i = 40$ meV and k_i parallel to the c axis. Unpolarized neutron scattering experiments were performed at the thermal neutron triple-axis spectrometer TAIPAN at Australian Centre for Neutron

Scattering, ANSTO, Australia, with fixed final energy $E_f = 14.7$ meV. The scattering plane $(H, 0, 0) \times (0, 0, L)$ is defined by using a pseudo-orthorhombic magnetic unit cell with $a_M \approx b_M \approx 5.52$ Å, $c_M = 10.27$ Å, and the vector \mathbf{Q} in reciprocal space is defined as $\mathbf{Q} = H\mathbf{a}^* + K\mathbf{b}^* + L\mathbf{c}^*$, where H , K , and L are Miller indices and $\mathbf{a}^* = \hat{\mathbf{a}}2\pi/a_M$, $\mathbf{b}^* = \hat{\mathbf{b}}2\pi/b_M$, $\mathbf{c}^* = \hat{\mathbf{c}}2\pi/c_M$ are reciprocal lattice units. Polarized neutron scattering experiments were carried out using the CryoPAD system at the CEA-CRG IN22 thermal triple-axis spectrometer of the Institut Laue-Langevin, Grenoble, France, with the same scattering plane and final energy as the TAIPAN experiment. We define the neutron polarization directions as x, y, z , with x parallel to \mathbf{Q} , and y and z perpendicular to \mathbf{Q} as shown in Fig. 1(c). At a specific momentum and energy transfer, magnetically scattered neutrons can have polarizations antiparallel [neutron spin flip (SF) $\uparrow\downarrow$] to the incident neutrons. The three neutron SF scattering cross sections can be written as $\sigma_\alpha^{\text{SF}}$, where $\alpha = x, y, z$. Since neutron scattering is only sensitive to those magnetic scattering components perpendicular to the momentum transfer \mathbf{Q} , we therefore have $\sigma_x^{\text{SF}} = cM_y + cM_z + B$, $\sigma_y^{\text{SF}} = cM_z + B$, $\sigma_z^{\text{SF}} = cM_y + B$, where M_y and M_z are the magnetic fluctuation moments along the y and z directions, B is the constant background from the instrument, and $c = (R - 1)/(R + 1)$ with spin flipping ratio $R \approx 15$ in our experiment [51–57]. If the spin excitations are completely isotropic in spin space, then M_y must be identical to M_z , resulting in $\sigma_y^{\text{SF}} = \sigma_z^{\text{SF}} = (\sigma_x^{\text{SF}} + B)/2$.

Figure 2 shows the energy and momentum dependence of low-energy spin excitations at 7 K (below T_c) and 30 K (above T_c) measured at HRC. A significant enhancement of the spin excitations from 8 to 15 meV is found at the superconducting state ($T = 7$ K), with an ellipse shape elongated along the K direction but no clear energy dispersion [Figs. 2(a)-2(d)]. By comparing the spin excitation intensity below and above T_c , a resonance mode is identified to be around 11 meV at the zone center $\mathbf{Q} = (1, 0)$ (Figs. 2(e) and 2(f)). Given $T_c = 22$ K, we have $E_R = 5.8k_B T_c$, which is close to the prefactor 4.9 as shown in Fig. 1(d) [37]. The momentum transfer and temperature dependence of the spin resonance is measured at TAIPAN, as shown in Figs. 3(a) and 3(b). For clarity, we only present the intensity differences between the superconducting and normal states. The spin excitations remain almost the same for different $L = 0.5, 0.75$, and 1 from 2 to 15 meV within the first Brillouin zone, suggesting the 2D nature of the resonance mode. Moreover, the resonance energy corresponding to the maximum intensity is nearly temperature independent; thus, it does not exactly follow the temperature dependence of the BCS-like superconducting gaps [15, 16, 58–64].

To further check the anisotropy of the spin resonance in energy, \mathbf{Q} , and the temperature dependence, we further carried out polarized neutron scattering at IN22. The

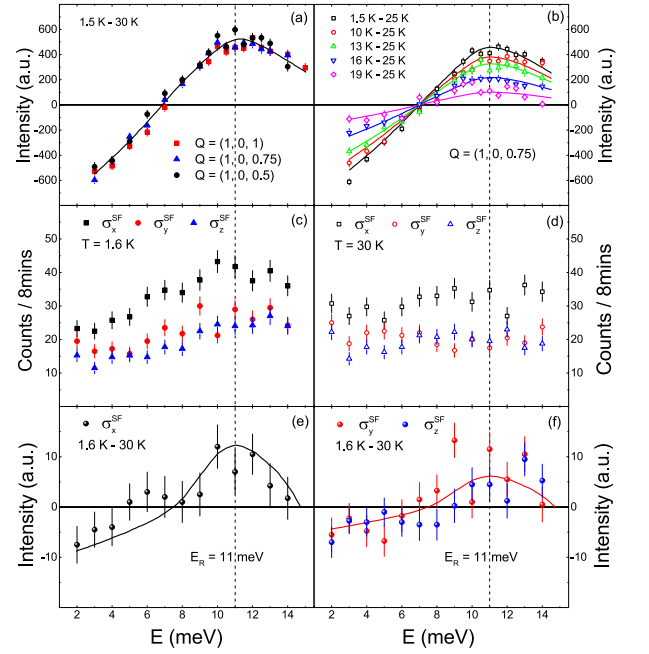


FIG. 3: (a) Energy dependence of the spin resonance at $\mathbf{Q} = (1, 0, L)$ with $L = 0.5, 0.75$, and 1 for unpolarized neutron scattering. (b) Temperature dependence of the spin resonance at $\mathbf{Q} = (1, 0, 0.75)$ from 1.5 to 19 K. (c)-(f) Energy scans at $\mathbf{Q} = (1, 0, 0.5)$ for SF scattering below and above T_c and their difference for each neutron polarization direction, marked as $\sigma_{x,y,z}^{\text{SF}}$. The solid lines in (a), (b), (d), and (e) are guides to the eyes, and in (f) the solid line is the half of (e).

raw data of the magnetic scattering in SF channels at $T = 1.6$ K (below T_c) and 30 K (above T_c) is shown in Figs. 3(c) and 3(d), respectively. There is no clear difference between σ_y^{SF} and σ_z^{SF} at both temperatures within error bars, suggesting isotropic spin excitations in both superconducting and normal states [51–53]. The difference of $\sigma_\alpha^{\text{SF}}$ ($\alpha = x, y, z$) at $\mathbf{Q} = (1, 0, 0.5)$ below and above T_c confirms the 11 meV resonance mode [Figs. 3(e) and 3(f)]. Since the temperature difference plots in Figs. 3(e) and 3(f) should contain no background, we expect $\sigma_x^{\text{SF}} = \sigma_y^{\text{SF}} + \sigma_z^{\text{SF}} = 2\sigma_y^{\text{SF}}$ [52]. The red line in Fig. 3(f) indicates the half intensity of σ_x^{SF} (black line) in Fig. 3(e), and it is indeed statistically identical to σ_y^{SF} or σ_z^{SF} .

Figures 4(a) and 4(b) summarize constant energy scans along the $(H, 0, 0.5)$ direction at the resonance energy $E_R = 11$ meV with different neutron polarizations. All three channels display well-defined Gaussian peaks both at $T = 1.6$ K and 30 K. After subtracting the flat background, the spin excitations are nearly isotropic by satisfying $\sigma_x^{\text{SF}} = 2\sigma_y^{\text{SF}} = 2\sigma_z^{\text{SF}}$, except for a negligible difference between σ_y^{SF} and σ_z^{SF} at the zone center with $T = 1.6$ K. Since the magnetic fluctuating moments can be expressed by $M_y = M_a \sin^2 \theta + M_c \cos^2 \theta$ and $M_z = M_b$ [θ is the angle between \mathbf{Q} and the $(H, 0, 0)$ directions]

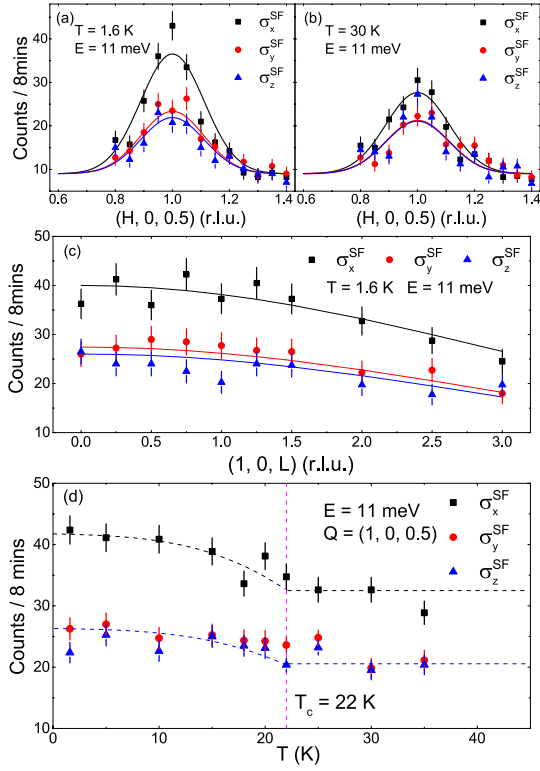


FIG. 4: (a), (b) Constant energy scans at $E = 11$ meV along $\mathbf{Q} = (H, 0, 0.5)$ in the neutron SF channel $\sigma_{x,y,z}^{\text{SF}}$ below and above T_c , respectively. The solid lines are Gaussian fits to the raw data. (c) Constant energy scans along $\mathbf{Q} = (1, 0, L)$ at $E = 11$ meV and $T = 1.6$ K. The solid lines represent the square of the form factor normalized by the initial intensity for each channel. (d) Temperature dependence of the neutron SF scattering cross section $\sigma_{x,y,z}^{\text{SF}}$ at $E = 11$ meV and $\mathbf{Q} = (1, 0, 0.5)$. The dashed lines are guides to the eyes.

[7, 52, 53, 57], and as we actually have $M_a = M_b$ due to the diagonal orientation of ordered moments [1, 47], the difference between M_y and M_z (σ_y^{SF} and σ_z^{SF}) must come from the anisotropic excitations between M_a and M_c and decrease with increasing L . It turns out to be not the case in our experiment, because all three channels of the spin resonance do not have either any clear modulation or an abnormal dependence besides the intensity following the square of the form factor $|f_M(\mathbf{Q})|^2$ ranging from $L = 0$ to $L = 3$ [Fig. 4(c)]. The small and persistent difference between σ_y^{SF} and σ_z^{SF} in Fig. 4(c) is attributed to the slight change of the flipping ratio in these two channels instead of the spin anisotropy. Finally, a temperature dependence of the spin resonance at all three neutron polarizations is shown in Fig. 4(d). The intensity of σ_x^{SF} likes an order parameter and responds to T_c , and the spin excitations are isotropic except for the perturbation from critical scattering around T_c [56, 57].

To figure out the band structure and fermiology in this particular compound, we performed generalized-gradient-approximation (GGA) calculations, as shown in

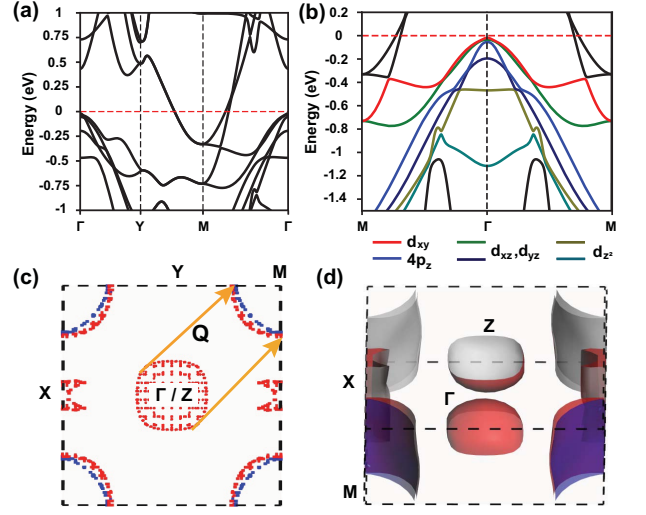


FIG. 5: (a), (b) Band structure and orbital occupation of $\text{Ca}_{0.82}\text{La}_{0.18}\text{Fe}_{0.96}\text{Ni}_{0.04}\text{As}_2$ from the GGA calculation. (c), (d) Fermi surfaces in 2D projection and 3D reciprocal space from the GGA calculation.

Fig. 5. Similar to the Ni free system $\text{Ca}_{1-x}\text{La}_x\text{FeAs}_2$, the As 4p orbitals are involved besides the Fe 3d orbitals (Figs. 5(a) and 5(b)), resulting in a 3D hole pocket around the Γ point and a small 2D electron pocket around the X point (Figs. 5(c) and 5(d)). The other 2D hole sheet outside the zone center, as shown in the dynamical mean field theory (DMFT) calculation of $\text{Ca}_{1-x}\text{La}_x\text{FeAs}_2$ [39, 41–43], is not found in our GGA calculation due to the Ni doping effect. Since we only find a 2D spin resonance around $\mathbf{Q} = (1, 0)$ (Fig. 2) corresponding to the wave vector \mathbf{Q} from Γ/Z to M [Fig. 5(c)], the extra electron pocket at the X point thus has no contribution to the spin excitations or superconductivity. The s_{\pm} pairing only happens on the 3D hole pocket around the Γ point and 2D electron pockets at the M point.

The complex multiorbital nature in iron-based superconductors may lead to a dispersion and spin anisotropy of the spin resonance [19, 52, 53, 64–71]. In a recent study on $\text{CaKFe}_4\text{As}_4$ (1144 compound), the spin resonance is found to be composed with nondispersive triple modes with energies scaling with the total superconducting gaps summed on the nesting hole and electron pockets. In contrast to its 2D fermiology, the resonance intensity has highly 3D modulation with both odd and even L symmetries due to the nondegenerate spin excitations from the Fe-As bilayer [26]. For our case in the 112 system, although the broad energy distribution of the spin resonance may be involved with multimodes due to the double electron sheets, the resonance energy and intensity is completely L independent, suggesting a 2D nature of the resonant mode despite the 3D hole pocket. Therefore, the spin resonance actually does not respond to the

k_z dependence of the fermiology in the iron-based superconductor. More uniquely for the 112 system, the spin-orbit coupling is rather weak due to the decoupled structural transition and magnetic transition in the “parent” compound [1, 39]; the Ni doping further weakens the orbital ordering as well as the nematicity [72, 73]. This fact enables us to reveal that the spin resonance intrinsically is an isotropic spin-1 collective mode of spin excitations. Moreover, the presence of additional zigzag As chains probably blocks the correlations for FeAs interlayers; then the Ni doping can eliminate the 3D AF order very easily [1], giving rise to a 2D superconductivity and spin resonance in the doped compounds [49, 74]. Finally, the nearly temperature independent resonance energy is also consistent with the $s\pm$ pairing mechanism [64].

In summary, inelastic neutron scattering experiments have been carried out on the 112-type iron pnictide superconductor $\text{Ca}_{0.82}\text{La}_{0.18}\text{Fe}_{0.96}\text{Ni}_{0.04}\text{As}_2$. A 2D spin resonance mode around $E = 11$ meV is found. The nearly temperature independent resonance energy scales with T_c along with other iron-based superconductors. The isotropic intensity of the resonance in spin space suggests that it is a spin-1 excited mode of Cooper pairs in the case of weak spin-orbital coupling. Comparing with our recent study on $\text{CaKFe}_4\text{As}_4$ [26], we argue that the spin resonance in the iron-based superconductor intrinsically is a spin singlet-triplet exciton and does not respond to the k_z dependence of the fermiology.

This work is supported by the National Natural Science Foundation of China (Grants No. 11374011, No. 11374346, No. 11674406, and No. 11674372), the National Key Research and Development Program of China (Grants No. 2017YFA0302903, No. 2017YFA0303103, No. 2016YFA0300502) and the Strategic Priority Research Program (B) of the Chinese Academy of Sciences (Grants No. XDB07020300, No. XDPB01). H. L. is supported by the Youth Innovation Promotion Association of CAS. A.G. is supported by HBNI, and H.G. gratefully acknowledges P. A. Naik, A. Banerjee for support. The neutron-scattering experiment at HRC was performed with the J-PARC (2016B0068).

* Electronic address: hqluo@iphy.ac.cn

[1] J. Rossat-Mignod, L.-P. Regnault, C. Vettier, P. Bourges, P. Bulet, J. Bossy, J. Y. Henry, and G. Lapertot, *Physica (Amsterdam)* **185C-189C**, 86 (1991).
 [2] N. K. Sato, N. Aso, K. Miyake, R. Shiina, P. Thalmeier, G. Varelogiannis, C. Geibel, F. Steglich, P. Fulde, and T. Komatsubara, *Nature (London)* **410**, 340 (2001).
 [3] S. D. Wilson, P. Dai, S. Li, S. Chi, H. J. Kang, and J. W. Lynn, *Nature (London)* **442**, 59 (2006).
 [4] A. D. Christianson, E. A. Goremychkin, R. Osborn, S. Rosenkranz, M. D. Lumsden, C. D. Malliakas, I. S. Todorov, H. Claus, D. Y. Chung, M. G. Kanatzidis, R. I. Bewley, and T. Guidi, *Nature (London)* **456**, 930 (2008).

[5] P. Dai, *Rev. Mod. Phys.* **87**, 855 (2015).
 [6] M. Eschrig, *Adv. Phys.* **55**, 47 (2006).
 [7] O. J. Lipscombe, L. W. Harriger, P. G. Freeman, M. Enderle, C. Zhang, M. Wang, T. Egami, J. Hu, T. Xiang, M. R. Norman, and P. Dai, *Phys. Rev. B* **82**, 064515 (2010).
 [8] S. Li, X. Lu, M. Wang, H. Q. Luo, M. Wang, C. Zhang, E. Faulhaber, L.-P. Regnault, D. Singh, and P. Dai, *Phys. Rev. B* **84**, 024518 (2011).
 [9] G. Yu, Y. Li, E. M. Motoyama, and M. Greven, *Nat. Phys.* **5**, 873 (2009).
 [10] D. S. Inosov, *C. R. Phys.* **17**, 60 (2016).
 [11] M. D. Lumsden, A. D. Christianson, D. Parshall, M. B. Stone, S. E. Nagler, G. J. MacDougall, H. A. Mook, K. Lokshin, T. Egami, D. L. Abernathy, E. A. Goremychkin, R. Osborn, M. A. McGuire, A. S. Sefat, R. Jin, B. C. Sales, and D. Mandrus, *Phys. Rev. Lett.* **102**, 107005 (2009).
 [12] S. Chi, A. Schneidewind, J. Zhao, L. W. Harriger, L. Li, Y. Luo, G. Cao, Z. Xu, M. Loewenhaupt, J. Hu, and P. Dai, *Phys. Rev. Lett.* **102**, 107006 (2009).
 [13] Y. Qiu, W. Bao, Y. Zhao, C. Broholm, V. Stanev, Z. Tesanovic, Y. C. Gasparovic, S. Chang, J. Hu, B. Qian, M. Fang, and Z. Mao, *Phys. Rev. Lett.* **103**, 067008 (2009).
 [14] H. A. Mook, M. D. Lumsden, A. D. Christianson, S. E. Nagler, B. C. Sales, R. Jin, M. A. McGuire, A. S. Sefat, D. Mandrus, T. Egami, and C. dela. Cruz, *Phys. Rev. Lett.* **104**, 187002 (2010).
 [15] D. S. Inosov, J. T. Park, P. Bourges, D. L. Sun, Y. Sidis, A. Schneidewind, K. Hradil, D. Haug, C. T. Lin, B. Keimer, and V. Hinkov, *Nat. Phys.* **6**, 178 (2010).
 [16] C. Zhang, M. Wang, H. Luo, M. Wang, M. Liu, J. Zhao, D. L. Abernathy, T. A. Maier, K. Marty, M. D. Lumsden, S. Chi, S. Chang, J. A. Rodriguez-Rivera, J. W. Lynn, T. Xiang, J. Hu, and P. Dai, *Sci. Rep.* **1**, 115 (2011).
 [17] M. Ishikado, Y. Nagai, K. Kodama, R. Kajimoto, M. Nakamura, Y. Inamura, S. Wakimoto, H. Nakamura, M. Machida, K. Suzuki, H. Usui, K. Kuroki, A. Iyo, H. Eisaki, M. Arai, and S. I. Shamoto, *Phys. Rev. B* **84**, 144517 (2011).
 [18] J. Zhao, C. R. Rotundu, K. Marty, M. Matsuda, Y. Zhao, C. Setty, E. Bourret-Courchesne, J. Hu, and R. J. Birge-neau, *Phys. Rev. Lett.* **110**, 147003 (2013).
 [19] C. H. Lee, P. Steffens, N. Qureshi, M. Nakajima, K. Kihou, A. Iyo, H. Eisaki, and M. Braden, *Phys. Rev. Lett.* **111**, 167002 (2013).
 [20] C. Zhang, R. Yu, Y. Su, Y. Song, M. Wang, G. Tan, T. Egami, J. A. Fernandez-Baca, E. Faulhaber, Q. Si, and P. Dai, *Phys. Rev. Lett.* **111**, 207002 (2013).
 [21] N. Qureshi, P. Steffens, Y. Drees, A. C. Komarek, D. Lamago, Y. Sidis, L. Harnagea, H.-J. Grafe, S. Wurmehl, B. Büchner, and M. Braden, *Phys. Rev. Lett.* **108**, 117001 (2012).
 [22] S. Wakimoto, K. Kodama, M. Ishikado, M. Matsuda, R. Kajimoto, M. Arai, K. Kakurai, F. Esaka, A. Iyo, H. Kito, H. Eisaki, and S. Shamoto, *J. Phys. Soc. Jpn.* **79**, 074715 (2010).
 [23] J. T. Park, G. Friemel, Yuan Li, J.-H. Kim, V. Tsurkan, J. Deisenhofer, H.-A. Krug von Nidda, A. Loidl, A. Ivanov, B. Keimer, and D. S. Inosov, *Phys. Rev. Lett.* **107**, 177005 (2011).
 [24] Q. Wang, Y. Shen, B. Pan, Y. Hao, M. Ma, F. Zhou, P. Steffens, K. Schmalzl, T. R. Forrest, M. Abdel-Hafez, X. Chen, D. A. Chareev, A. N. Vasiliev, P. Bourges, Y. Sidis, H. Cao, and J. Zhao, *Nat. Mater.* **15**, 159 (2016).
 [25] K. Iida, M. Ishikado, Y. Nagai, H. Yoshida, A. D. Chris-

- tianson, N. Murai, K. Kawashima, Y. Yoshida, H. Eisaki, and A. Iyo, *J. Phys. Soc. Jpn.* **86**, 093703 (2017).
- [26] T. Xie, Y. Wei, D. Gong, T. Fennell, U. Stuhr, R. Kajimoto, K. Ikeuchi, S. Li, J. Hu, and H. Luo, arXiv:1802.01901.
- [27] M. Ma, L. Wang, P. Bourges, Y. Sidis, S. Danilkin, and Y. Li, *Phys. Rev. B* **95**, 100504 (2017).
- [28] M. Sato, T. Kawamata, Y. Kobayashi, Y. Yasui, T. Iida, K. Suzuki, M. Itoh, T. Moyoshi, K. Motoya, R. Kajimoto, M. Nakamura, Y. Inamura, and M. Arai, *J. Phys. Soc. Jpn.* **80**, 093709 (2011).
- [29] Q. Wang, J. T. Park, Y. Feng, Y. Shen, Y. Hao, B. Pan, J. W. Lynn, A. Ivanov, S. Chi, M. Matsuda, H. Cao, R. J. Birgeneau, D. V. Efremov, and J. Zhao, *Phys. Rev. Lett.* **116**, 197004 (2016).
- [30] M. A. Surmach, F. Brückner, S. Kamusella, R. Sarkar, P. Y. Portnichenko, J. T. Park, G. Ghambashidze, H. Luetkens, P. K. Biswas, W. J. Choi, Y. I. Seo, Y. S. Kwon, H.-H. Klauss, and D. S. Inosov, *Phys. Rev. B* **91**, 104515 (2015).
- [31] K. Ikeuchi, M. Sato, R. Kajimoto, Y. Kobayashi, K. Suzuki, M. Itoh, P. Bourges, A. D. Christianson, H. Nakamura, and M. Machida, *JPS Conf. Proc.* **3**, 015043 (2014).
- [32] C. H. Lee, K. Kihou, J. T. Park, K. Horigane, K. Fujita, F. Waßer, N. Qureshi, Y. Sidis, J. Akimitsu, and M. Braden, *Sci. Rep.* **6**, 23424 (2016).
- [33] I. I. Mazin, D. J. Singh, M. D. Johannes, and M. H. Du, *Phys. Rev. Lett.* **101**, 057003 (2008).
- [34] K. Kuroki, S. Onari, R. Arita, H. Usui, Y. Tanaka, H. Kontani, and H. Aoki, *Phys. Rev. Lett.* **101**, 087004 (2008).
- [35] H. Ding, P. Richard, K. Nakayama, K. Sugawara, T. Arakane, Y. Sekiba, A. Takayama, S. Souma, T. Sato, and T. Takahashi, *Europhys. Lett.* **83**, 47001 (2008).
- [36] M. Wang, H. Luo, J. Zhao, C. Zhang, M. Wang, K. Marty, S. Chi, J. W. Lynn, A. Schneidewind, S. Li, and P. Dai, *Phys. Rev. B* **81**, 174524 (2010).
- [37] P. D. Johnson, G. Xu, and W. -G. Yin *Iron-Based Superconductivity*, (Springer, New York, 2015), pp 165-169.
- [38] N. Katayama, K. Kudo, S. Onari, T. Mizukami, K. Sugawara, Y. Sugiyama, Y. Kitahama, K. Iba, K. Fujimura, N. Nishimoto, M. Nohara, and H. Sawa, *J. Phys. Soc. Jpn.* **82**, 123702 (2013).
- [39] S. Jiang, C. Liu, H. Cao, T. Birol, J. M. Allred, W. Tian, L. Liu, K. Cho, M. J. Krogstad, J. Ma, K. M. Taddei, M. A. Tanatar, M. Hoesch, R. Prozorov, S. Rosenkranz, Y. J. Uemura, G. Kotliar, and N. Ni, *Phys. Rev. B* **93**, 054522 (2016).
- [40] T. Xie, D. Gong, W. Zhang, Y. Gu, Z. Huesges, D. Chen, Y. Liu, L. Hao, S. Meng, Z. Lu, S. Li, and H. Luo, *Supercond. Sci. Technol.* **30**, 095002 (2017).
- [41] X. Liu, D. Liu, L. Zhao, Q. Guo, Q. Mu, D. Chen, B. Shen, H. Yi, J. Huang, J. He, Y. Peng, Y. Liu, S. He, G. Liu, X. Dong, J. Zhang, C. Chen, Z. Xu, Z. Ren, and X. Zhou, *Chin. Phys. Lett.* **30**, 127402 (2013).
- [42] M. Y. Li, Z. T. Liu, W. Zhou, H. F. Yang, D. W. Shen, W. Li, J. Jiang, X. H. Niu, B. P. Xie, Y. Sun, C. C. Fan, Q. Yao, J. S. Liu, Z. X. Shi, and X. M. Xie, *Phys. Rev. B* **91**, 045112 (2015).
- [43] Z. Liu, X. Xing, M. Li, W. Zhou, Y. Sun, C. Fan, H. Yang, J. Liu, Q. Yao, W. Li, Z. Shi, D. Shen, and Z. Wang, *Appl. Phys. Lett.* **109**, 042602 (2016).
- [44] H. Yakita, H. Ogino, T. Okada, A. Yamamoto, K. Kishio, T. Tohei, Y. Ikuhara, Y. Gotoh, H. Fujihisa, K. Kataoka, H. Eisaki, and J. Shimoyama, *J. Am. Chem. Soc.*, **136**, 846 (2014).
- [45] H. Ota, K. Kudo, T. Kimura, Y. Kitahama, T. Mizukami, S. Ioka, and M. Nohara, *J. Phys. Soc. Jpn.* **86**, 025002 (2017).
- [46] S. Kawasaki, T. Mabuchi, S. Maeda, T. Adachi, T. Mizukami, K. Kudo, M. Nohara, and G. Q. Zheng, *Phys. Rev. B* **92**, 180508 (2015).
- [47] S. Jiang, L. Liu, M. Schütt, A. M. Hallas, B. Shen, W. Tian, E. Emmanouilidou, A. Shi, G. M. Luke, Y. J. Uemura, R. M. Fernandes, and N. Ni, *Phys. Rev. B* **93**, 174513 (2016).
- [48] Z. Wang, T. Xie, E. Kampert, T. Förster, X. Lu, R. Zhang, D. Gong, S. Li, T. Herrmannsdörfer, J. Wosnitza, and H. Luo, *Phys. Rev. B* **92**, 174509 (2015).
- [49] D. Sónora, C. Carballeira, J. J. Ponte, T. Xie, H. Luo, S. Li, and J. Mosqueira, *Phys. Rev. B* **96**, 014516 (2017).
- [50] See Supplemental Material, which includes the sample photo and characterizations.
- [51] M. Liu, C. Lester, J. Kulda, X. Lu, H. Luo, M. Wang, S. M. Hayden, and P. Dai, *Phys. Rev. B* **85**, 214516 (2012).
- [52] H. Luo, M. Wang, C. Zhang, X. Lu, L.-P. Regnault, R. Zhang, S. Li, J. Hu, and P. Dai, *Phys. Rev. Lett.* **111**, 107006 (2013).
- [53] D. Hu, W. Zhang, Y. Wei, B. Roessli, M. Skoulatos, L.-P. Regnault, G. Chen, Y. Song, H. Luo, S. Li, and P. Dai, *Phys. Rev. B* **96**, 180503(R) (2017).
- [54] C. Wang, R. Zhang, F. Wang, H. Luo, L.-P. Regnault, P. Dai, and Y. Li, *Phys. Rev. X* **3**, 041036 (2013).
- [55] N. Qureshi, P. Steffens, S. Wurmehl, S. Aswartham, B. Büchner, and M. Braden, *Phys. Rev. B* **86**, 060410(R) (2012).
- [56] Y. Song, W. Wang, C. Zhang, Y. Gu, X. Lu, G. Tan, Y. Su, F. Bourdarot, A. D. Christianson, S. Li, and P. Dai, *Phys. Rev. B* **96**, 184512 (2017).
- [57] Y. Song, L.-P. Regnault, C. Zhang, G. Tan, S. V. Carr, S. Chi, A. D. Christianson, T. Xiang, and P. Dai, *Phys. Rev. B* **88**, 134512 (2013).
- [58] L. W. Harriger, O. J. Lipscombe, C. Zhang, H. Luo, M. Wang, K. Marty, M. D. Lumsden, and P. Dai, *Phys. Rev. B* **85**, 054511 (2012).
- [59] H. Luo, X. Lu, R. Zhang, M. Wang, E. A. Goremychkin, D. T. Adroja, S. Danilkin, G. Deng, Z. Yamani, and P. Dai, *Phys. Rev. B* **88**, 144516 (2013).
- [60] I. I. Mazin and J. Schmalian, *Physica (Amsterdam)* **469C**, 614 (2009).
- [61] T. A. Maier and D. J. Scalapino, *Phys. Rev. B* **78**, 020514(R) (2008).
- [62] T. A. Maier, S. Graser, D. J. Scalapino, and P. Hirschfeld, *Phys. Rev. B* **79**, 134520 (2009).
- [63] M. M. Korshunov and I. Eremin, *Phys. Rev. B* **78**, 140509(R) (2008).
- [64] C. Zhang, H. F. Li, Y. Song, Y. Su, G. Tan, T. Netherton, C. Redding, S. V. Carr, O. Sobolev, A. Schneidewind, E. Faulhaber, L. W. Harriger, S. Li, X. Lu, D. X. Yao, T. Das, A. V. Balatsky, Th. Brückel, J. W. Lynn, and P. Dai, *Phys. Rev. B* **88**, 064504 (2013).
- [65] M. Wang, M. Yi, H. L. Sun, P. Valdivia, M. G. Kim, Z. J. Xu, T. Berlijn, A. D. Christianson, Songxue Chi, M. Hashimoto, D. H. Lu, X. D. Li, E. Bourret-Courchesne, Pengcheng Dai, D. H. Lee, T. A. Maier, and R. J. Birgeneau, *Phys. Rev. B* **93**, 205149 (2016).
- [66] P. Steffens, C. H. Lee, N. Qureshi, K. Kihou, A. Iyo, H. Eisaki, and M. Braden, *Phys. Rev. Lett.* **110**, 137001

- (2013).
- [67] C. Zhang, Y. Song, L.-P. Regnault, Y. Su, M. Enderle, J. Kulda, G. Tan, Z. C. Sims, T. Egami, Q. Si, and P. Dai, *Phys. Rev. B* **90**, 140502(R) (2014).
- [68] W. Wang, J. T. Park, R. Yu, Y. Li, Y. Song, Z. Zhang, A. Ivanov, J. Kulda, and P. Dai, *Phys. Rev. B* **95**, 094519 (2017).
- [69] P. Babkevich, B. Roessli, S. N. Gvasaliya, L.-P. Regnault, P. G. Freeman, E. Pomjakushina, K. Conder, and A. T. Boothroyd, *Phys. Rev. B* **83**, 180506(R) (2011).
- [70] M. Ma, P. Bourges, Y. Sidis, Y. Xu, S. Li, B. Hu, J. Li, F. Wang, and Y. Li, *Phys. Rev. X* **7**, 021025 (2017).
- [71] Y. Song, H. Man, R. Zhang, X. Lu, C. Zhang, M. Wang, G. Tan, L.-P. Regnault, Y. Su, J. Kang, R. M. Fernandes, and P. Dai, *Phys. Rev. B* **94**, 214516 (2016).
- [72] Y. Gu, Z. Liu, T. Xie, W. Zhang, D. Gong, D. Hu, X. Ma, C. Li, L. Zhao, L. Lin, Z. Xu, G. Tan, G. Chen, Z. Y. Meng, Y. F. Yang, H. Luo, and S. Li, *Phys. Rev. Lett.* **119**, 157001(2017).
- [73] C. -J. Kang, T. Birol, and G. Kotliar, *Phys. Rev. B* **95**, 014511 (2017).
- [74] X. Xing, W. Zhou, N. Zhou, F. Yuan, Y. Pan, H. Zhao, X. Xu, and Z. Shi, *Supercond. Sci. Technol.* **29**, 055005 (2016).

Supplementary Materials

We prepared high quality single crystals of $\text{Ca}_{0.82}\text{La}_{0.18}\text{Fe}_{0.96}\text{Ni}_{0.04}\text{As}_2$ using self-flux method, the detailed procedure of the crystal growth is shown in our previous report [1]. The size scale of the crystals is about 1 to 6 mm. We co-aligned 2.3 g single crystals (about 1500 pieces) by a X-ray Laue camera (*Photonic Sciences*) in backscattering mode with incident beam along c -axis. A hydrogen-free glue named *CYTOP* was painted on the back side of the crystals by sticking on thin aluminium plates and baked for 1-2 hours at 100 °C. The scattering plane was set up as $(H, 0, 0) \times (0, 0, L)$ with several aluminium plates with samples (Fig. S1). The neutron diffraction measurements on the whole sample array reveal a small mosaic of these co-aligned crystals. The rocking curves can be well fitted by Gaussian functions with full-width-at-half-maximum (FWHM) less than 3.7° for ab -plane ($Q = (2, 0, 0)$) and 2.8° along c -axis ($Q = (0, 0, 4)$) (Fig. S2).

Figure S3(a) shows the normalized resistivity

(ρ/ρ_{300K}) of our $\text{Ca}_{0.82}\text{La}_{0.18}\text{Fe}_{0.96}\text{Ni}_{0.04}\text{As}_2$ crystals. The sharp superconducting transitions, uniform T_c and nearly identical normal state behaviors among 8 randomly selected samples indicate high quality and homogeneity of our samples. No kinks of ρ related to the structural or magnetic transition can be found. Figure S3(b) shows the temperature dependence of the DC magnetic susceptibility for 2 typical crystals picked up from the resistivity measurements. The superconducting transitions are very sharp, and both of the samples have full Meissner shielding volume ($4\pi\chi \approx -1$) at based temperature ($T = 2$ K), suggesting bulk superconductivity in our crystals.

* Electronic address: hqluo@iphy.ac.cn

[1] T. Xie, D. Gong, W. Zhang, Y. Gu, Z. Huesges, D. Chen, Y. Liu, L. Hao, S. Meng, Z. Lu, S. Li, and H. Luo, *Supercond. Sci. Technol.* **30**, 095002 (2017).



FIG. S1: Photos of the assembled $\text{Ca}_{0.82}\text{La}_{0.18}\text{Fe}_{0.96}\text{Ni}_{0.04}\text{As}_2$ crystals on for neutron scattering experiments.

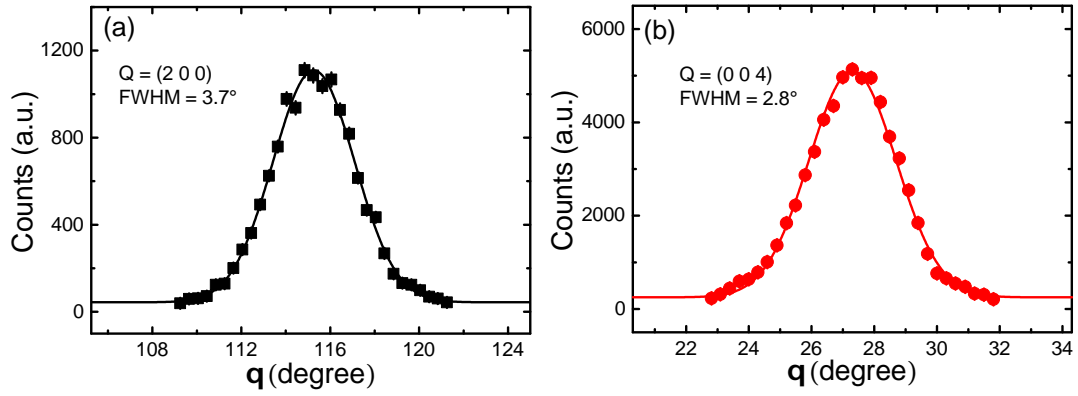


FIG. S2: Rocking curves of co-aligned crystals measured by neutron diffraction experiments. The solid lines are Gaussian fits of the data.

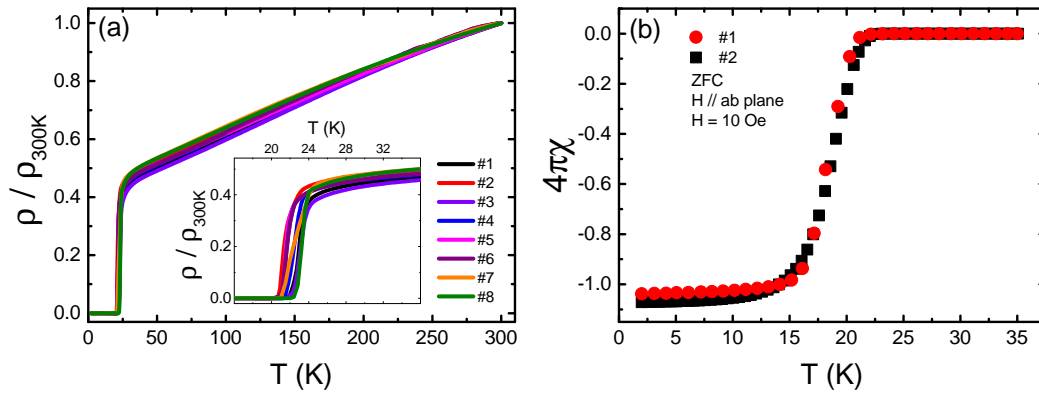


FIG. S3: Transport characterizations of our single crystals: (a) Temperature dependence of the resistivity, all the data is normalized by the resistivity at 300 K; (b) Temperature dependence of DC magnetic susceptibility.